Proceedings of the ASME 2023
International Mechanical Engineering Congress and Exposition
IMECE2023
October 29-November 2, 2022, New Orleans, Louisiana

IMECE2023-114306

A STUDY ON SURFACE TEXTURE AND WETTABILITY OF FEMTOSECOND LASER TREATED ALUMINUM ALLOY

Dakota Angell
Department of Industrial and Manufacturing Systems Engineering, Kansas State University
Manhattan, KS

Xinya Wang
Department of Industrial and Manufacturing Systems Engineering, Kansas State University
Manhattan, KS

Xiaoxu Song
Department of Industrial and Manufacturing Systems Engineering, Kansas State University
Manhattan, KS

Shuting Lei
Department of Industrial and Manufacturing Systems Engineering, Kansas State University
Manhattan, KS

ABSTRACT

This study aims to investigate the effects of femtosecond laser treatment on surface texture and wettability properties of an aluminum alloy, AL6061, with the primary goal of creating a superhydrophobic surface. A central composite design is used for the laser surface texturing design of experiments. Surface texture is examined using SEM to detect minuscule changes on the morphology. A 3D optical profiler extracts topographical data from the surface. A contact angle goniometer based on the sessile drop method is used to measure the contact angle of the textured samples. The response surface method is used to build a second-order polynomial model for the contact angle and obtain optimal parameters to maximize the contact angle. This research shows that laser surface texturing can generate a wide range of surface profiles and roughness values with geometric features ranging from hundreds of μm to submicron. All three laser parameters (pulse energy, pulse duration, pulse repetition rate) affect surface roughness and contact angle to some degree. To quantify the relationship between the contact angle and laser parameters, a response surface model for Al6061 is identified and used to find the optimal conditions of E=214 μJ, tp=10 ps, and fp=2427 Hz with a predicted maximum contact angle of 161°. A confirmation experiment produces a contact angle of 168°, in good agreement with the predicted value.

Keywords: laser surface texturing, aluminum alloy, surface wettability, response surface method

1. INTRODUCTION

Industrial use of femtosecond laser surface modification ranges from a variety of applications as well as material use. Metals such as aluminum and stainless steel are used in aerospace, annular pipes, and metallic molds. Thus, experimenting with these materials is common when treating the surface with femtosecond lasers. The goal to achieve surface wettability properties of hydrophobicity/superhydrophobicity is due to its potential applications in various fields such as self-cleaning, anti-icing, drag reduction, and more [1]. Aluminum has shown exciting results after being irradiated and appears to have less regular surface microcones than other metals such as stainless steel [2]. The varying results of surface microcones affect the surface properties and reactions towards various testing like wettability and surface free energy factors, giving reason to study further the results of femtosecond laser treated aluminum and stainless-steel surfaces. Various approaches target the desired surface outcomes and reproducibility in surface wettability when using a femtosecond laser. The general strategy reported in the literature includes surface microstructure alteration [3] and the combination of surface texturing and surface coating/chemical treatment to achieve either hydrophilic or hydrophobic surfaces [4,5].

Research suggests that laser texturing alone can control the wettability behavior of a material through surface morphology [6]. Research in recent years seems to indicate that a hierarchical structure consisting of micro and nano features created by ultrafast lasers can display superhydrophobic behavior [7,8], like the well-known structure of a lotus leaf in nature. Because surface oxidation after laser treatment often turns a metallic surface to superhydrophilic, low temperature annealing can be used after laser texturing to avert this adverse effect [9,10]. This study aims to develop a laser surface texturing technique in

© 2023 by ASME

combination with low temperature annealing to create a superhydrophobic surface made of AL6061, an aluminum alloy. A central composite design of experiments and response surface analysis are used to study the effects of laser treatment on the contact angle, a measure of the wettability property. The response surface analysis will offer directions to maximize contact angle by optimizing laser parameters. The overall workflow for this study is described as follows. It starts with laser surface texturing through the central composite design of experiments. The textured samples are then examined using a 3D profiler and SEM microscopy. Next, the samples undergo low temperature annealing at 200 °C for 2 hours. Finally, the response surface method is used to optimize the laser parameters to maximize the contact angle.

2. EXPERIMENTAL METHOD

2.1 CCD and Laser Processing Conditions

Central composite designs (CCD) are the most used response surface methodology. CCD is a factorial or fractional factorial design with center points, augmented with a group of axial points (also known as star points) that let one efficiently estimate the first and second-order terms [11]. A CCD always contains twice as many axial points as there are factors in the design. Axial points represent new extreme values (low and high) for each factor in the design. CCD is used in this research to determine the best conditions of laser parameters to produce superhydrophobic surfaces. The specific type of CCD used in this research is face centered. For face-centered CCD, star points are at the center of each face of the factorial space. This variety contains five levels for each factor. The figure below visually represents the face centered CCD.

The factors are pulse energy, pulse duration, and pulse repetition rate. Pulse energy, E (μJ), is the total optical energy content within a pulse. Pulse duration, tp (ps), is the duration of the laser pulse emitted on the sample. Pulse repetition rate, fp (Hz), is the frequency of pulses. These three factors are laser parameters that have a greater impact on the outcome of the surface than other laser parameters.

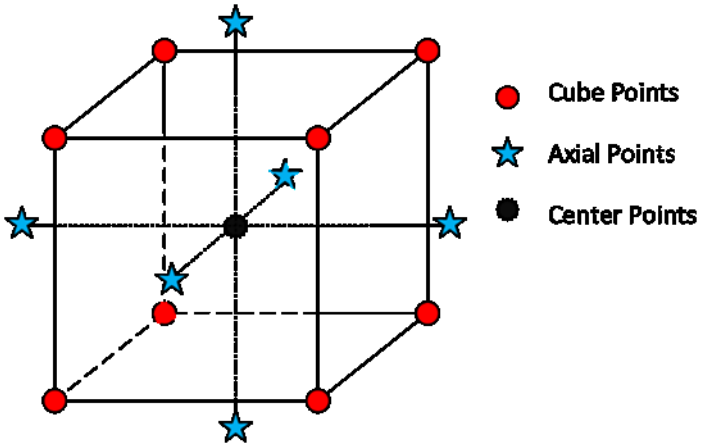

FIGURE 1: FACE CENTERED CCD DESIGN

The five factor levels in the CCD design are determined by the capability of the laser and some preliminary laser surface texturing experiments. For each of the three factors of the CCD design, the five levels are determined by multiplying the center point values by -1.68, -0.68, 0, 0.68, 1 for the factor levels of lowest, low, center, high, and highest, respectively. Table 1 below lists the three factors and five levels for each factor.

TABLE 1 CCD FACTOR AND FACTOR LEVELS

Factors	Factor levels				
	Lowest	Low	Center	High	Highest
E (μJ)	50	120	225	330	400
tp (ps)	0.184	2	5	8	10
fp (Hz)	400	1130	2200	3270	4000

This design has three sets of points: axial, cube, and center. Axial points represent the factor levels from the center value to the lowest or highest values for each factor, resulting in 6 different points; these points are run orders 1, 3, 8, 9, 10, and 19 in Table 2. Cube points represent the low and high factor levels resulting in 8 different points; these points are 2, 4, 7, 13, 14, 15, 18, and 20 in Table 2. Center points represent the factor level center and are repeated 6 times throughout; these points are 5, 6, 11, 12, 16, and 17 in Table 2. Run order 0 represents the as-received sample that is free from any laser treatment.

TABLE 2 CCD LASER CONDITIONS

Run order	E (μJ)	tp (ps)	fp (Hz)
0	as-received sample		
1	50	5	2200
2	330	2	1130
3	225	5	4000
4	120	8	3270
5	225	5	2200
6	225	5	2200
7	120	2	3270
8	225	0.184	2200
9	225	5	400
10	400	5	2200
11	225	5	2200
12	225	5	2200
13	330	8	1130
14	330	8	3270
15	330	2	3270
16	225	5	2200
17	225	5	2200
18	120	2	1130
19	225	10	2200
20	120	8	2200

© 2023 by ASME

2.2 Experimental Setup

The experimental setup for laser surface texturing is schematically shown in Figure 2. The ultrafast laser has pulse durations ranging from 184 fs to 10 ps. Pulse energy is adjusted by a half-wave plate and a cube polarizer. A focusing lens concentrates the pulse energy to a focal spot on the sample surface - the sample on a motorized xyz stage, controlled by the computer. Surface texturing is done through a continuous laser scan in the horizontal direction with constant stepping in the vertical direction.

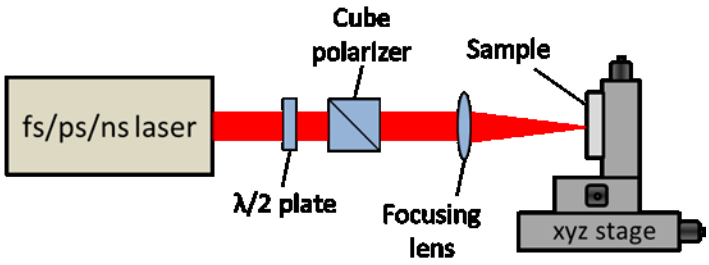

FIGURE 2: SCHEMATIC OF LASER SURFACE TEXTURING EXPERIMENTAL SETUP

The sample material is aluminum alloy 6061, a precipitation-hardened aluminum alloy containing magnesium and silicon as its major alloying elements [12]. This material has good mechanical properties, exhibits good weldability, and is one of the most common aluminum alloys for general-purpose use. Aluminum alloy 6061 is one of the most versatile of the heat-treatable alloys and is popular for medium to high strength requirements, exhibiting good toughness characteristics [13]. Its applications range from transportation components to machinery and equipment applications while exhibiting excellent corrosion resistance to atmospheric conditions [13].

Laser surface texturing experiments conducted follow the CCD design as described in Section 2.1. To shorten the time required for metal's wettability transition from hydrophilicity to superhydrophobicity without requiring the use of any chemical coating process, an additional process of annealing is introduced [9]. Annealing is performed in a conventional oven under ambient air at 200°C for 2 hours. The samples are treated usually within one day after laser surface texturing. No cleaning is done to the samples before annealing. Scanning electron microscope (SEM) is used to examine the surface microstructure after laser texturing. A 3D optical profiler is used to gather surface roughness values of the samples.

A standardized method is used during each measurement to gather surface wettability data. Prior to annealing, the wettability of the sample is measured daily once treated by the fs laser. As time passed, these measurements have become weekly, with slight change detected. Before annealing, the wettability of the sample is measured in three separate locations with a deionized water droplet of 2 μL. The purpose of measuring in three separate locations is to determine if the wettability remains consistent throughout the treated surface.

3. RESULTS AND DISCUSSION

The purpose of this section is to learn about laser parameters, surface microstructure, surface roughness, and wettability to see if there are any correlations. First, conditions relating to one factor at a time are selected based on the CCD design. One of the laser parameters will change by exploring one factor at a time. In contrast, the other two laser parameters remain at a fixed reference value (e.g., pulse energy at 225 μJ, pulse duration at 5 ps, and pulse repetition rate at 2200 Hz). The discussion is following cause-effect relationships: effects of laser parameters on surface texture, effects of laser parameters on surface roughness, effects of laser parameters on the contact angle, and effects of surface roughness on contact angle. Second, utilizing all the 20 test runs from the CCD design, response surface analysis will be used to establish a regression model relating laser parameters to contact angle.

3.1 Effects of Laser Parameters on Surface Texture

Surface textures presented in this section represent the wide range of surface morphology and profiles created in this study. These samples are grouped here to show the effects of the three laser parameters. Figure 3 shows three SEM images of laser textured Al6061 samples and the corresponding 3D profile images, with increasing pulse energy while keeping the other two parameters constant (pulse duration at 5 ps and pulse repetition rate at 2200 Hz). As the pulse energy increases, the number of asperities also increases, as seen in Figures 3b, 3d, and 3f. When the pulse energy is at 50 μJ there are few growths on the sample ranging from 1 μm to 3.5 μm in height. As pulse energy increases to 400 μJ, the surface not only has growth ranging from 5 μm to 20 μm but also has more material being displaced or ablated. The particle size appears to increase in proportion with pulse energy. At the highest pulse energy of 400 μJ, Al6061 appears to have columnar growth and splitting compared to the lowest pulse energy of 50 μJ, which appears to have little displaced material or ablation, as shown in Figures 3a and 3e. Multiscale features down to submicron levels are induced on the surface by laser irradiation.

© 2023 by ASME

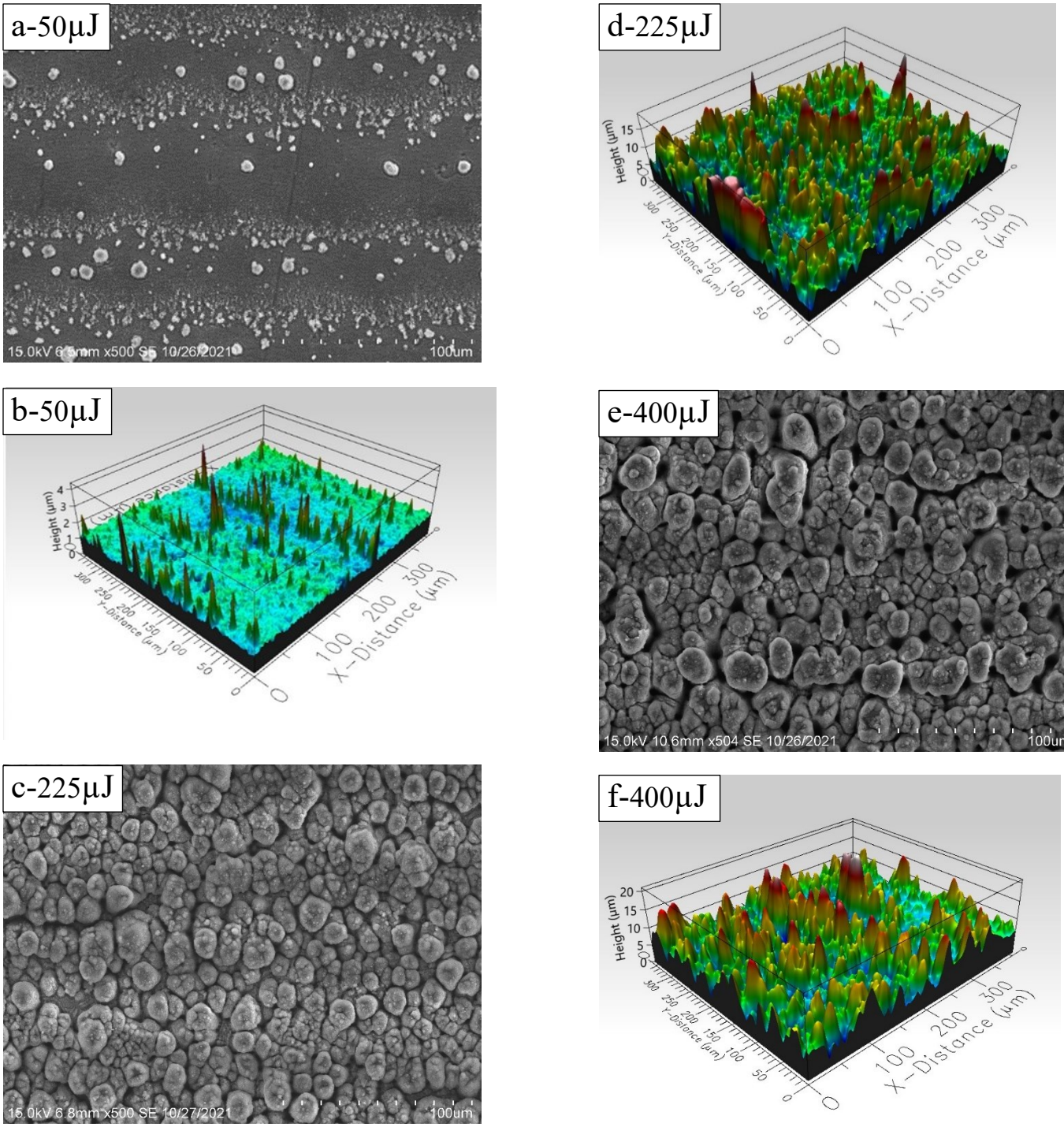

FIGURE 3: SEM IMAGES AND 3D PROFILES SHOWING THE EFFECTS OF PULSE ENERGY ON SURFACE TEXTURE

Figure 4 shows the SEM images and the 3D surface profiles for three laser textured surfaces of Al 6061. Of these images, pulse duration increases from 0.184 ps to 10 ps. Pulse duration shows an exciting trend, unlike that of pulse energy. It appears that the pulse duration effect plateaus at 5 ps. To further explain,

© 2023 by ASME

Figure 4a and Figure 4e are far more like each other; both appear to have material that is not deformed, ablated, or displaced. At the same time, Figure 4c appears to have more material deformed, ablated, and displaced. Figure 4b shows the most columnar growth, and Figures 4d and 4f have fewer growth or mounds of displaced material and less columnar growth. However, in Figures 4b, 4d, and 4f, growths and mounds of displaced material all seem to range in height from 0 µm to 15 µm.

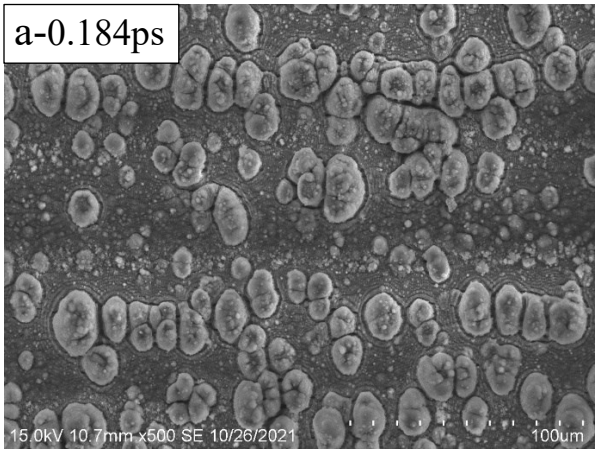

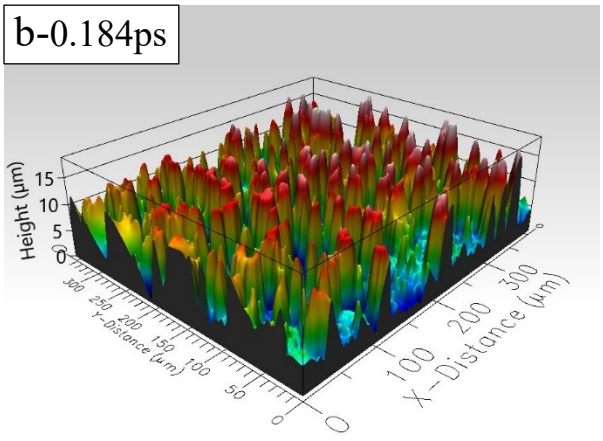

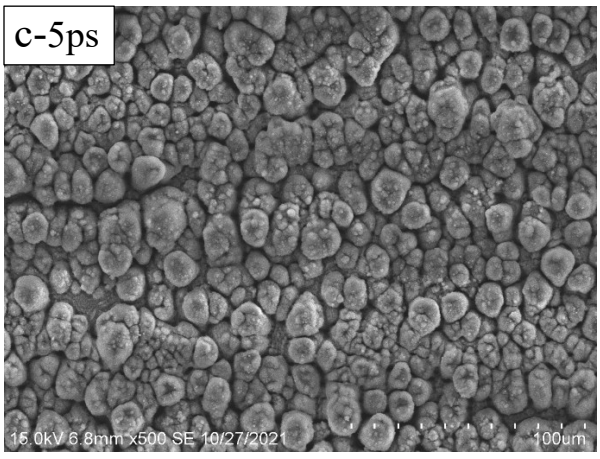

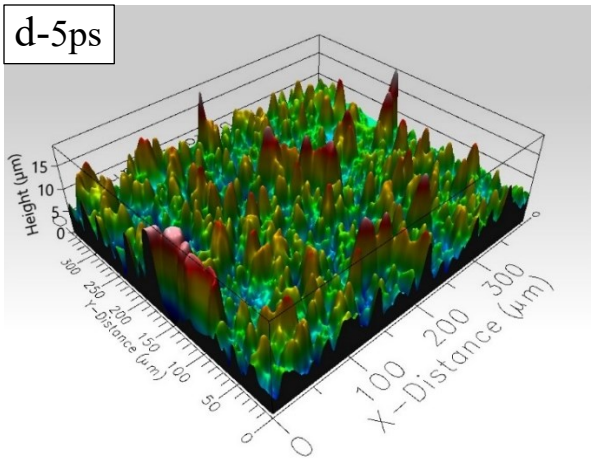

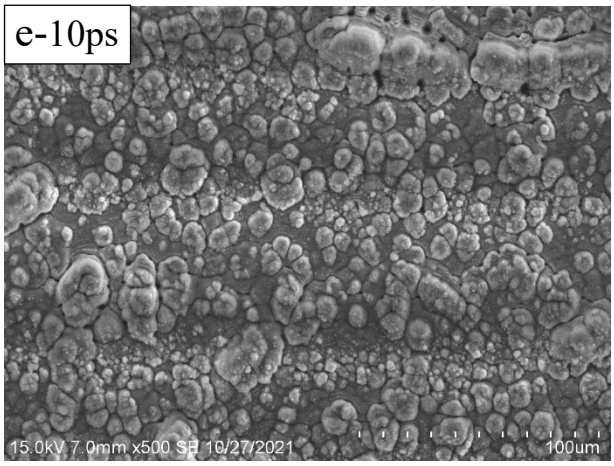

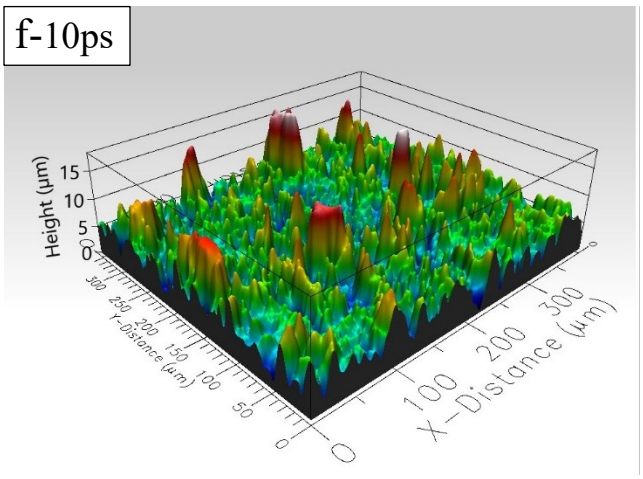

FIGURE 4: SEM IMAGES AND 3D PROFILES SHOWING THE EFFECTS OF PULSE DURATION ON SURFACE TEXTURE

Figure 5 shows the SEM images and the 3D surface profiles for three laser textured surfaces of Al 6061. Figures 5a and 5b show results of pulse repetition rate being at 400 Hz, while Figures 5c and 5d show results of pulse repetition rate being at 2200 Hz, and Figures 5e and 5f show results of pulse repetition

© 2023 by ASME

rate being at 4000 Hz, ten times the pulse repetition rate as Figures 5a and 5b. From observing the SEM images, Figures 5a, 5c, and 5e, it is apparent that the material changes by ablation, deformation, and displacement to an increasing extent as the pulse repetition rate increases. Figure 5a shows small areas of displaced material and has the most uniform surface compared to Figures 5c and 5e. There also seems to be more material showing columnar growth with an increasing repetition rate, as seen in Figures 5c and 5e. Surface pillars exhibit a more significant height difference reaching 20 μm at high repetition rates, as seen in Figures 5d and 5f, while Figure 5b shows growth reaching the height of only 1.5 μm.

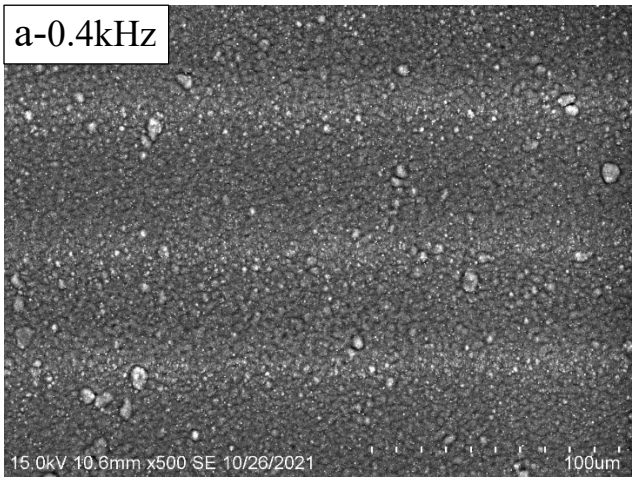

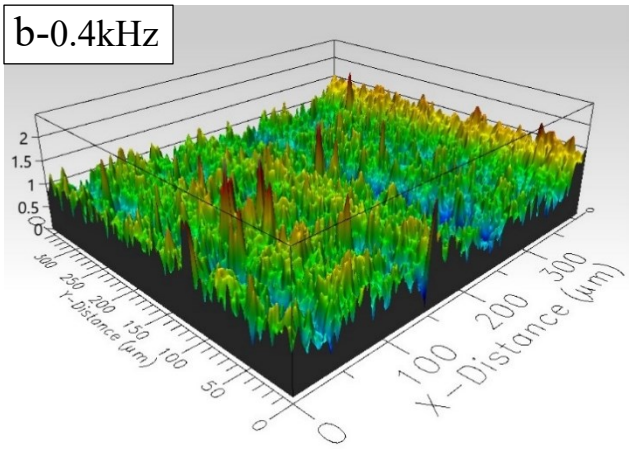

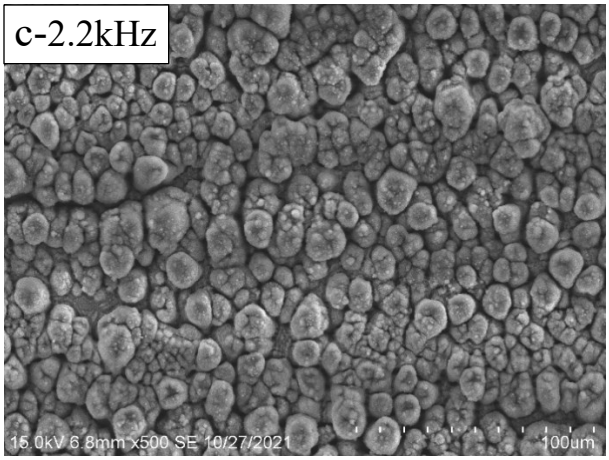

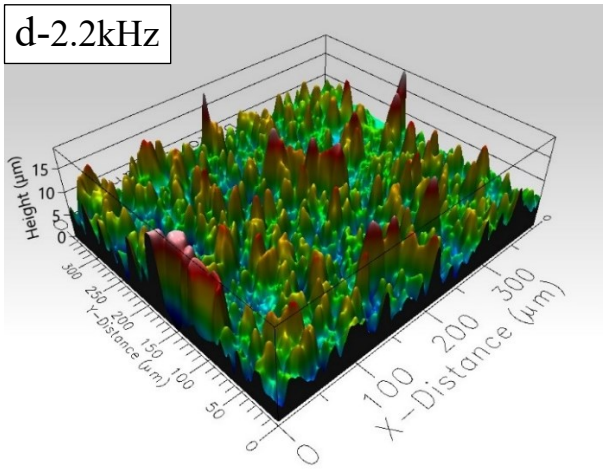

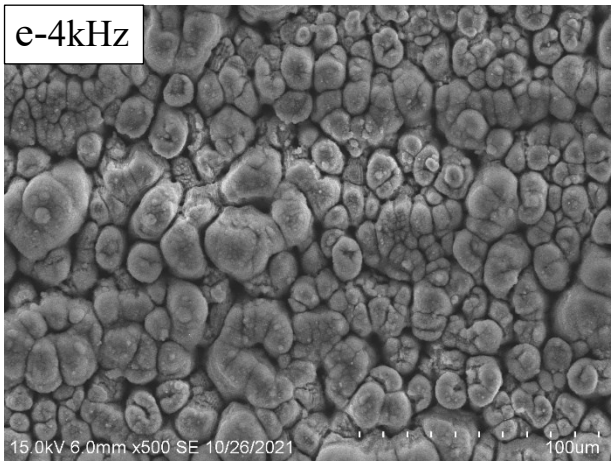

© 2023 by ASME

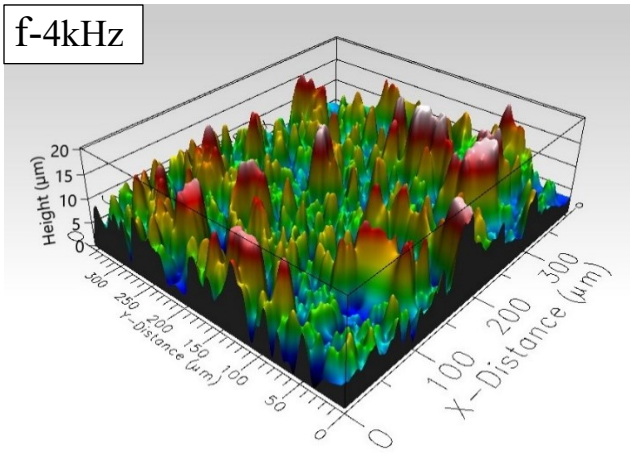

FIGURE 5: SEM IMAGES AND 3D PROFILES SHOWING THE EFFECTS OF PULSE REPETITION RATE ON SURFACE TEXTURE

3.2 Effects of Laser Parameters on Surface Roughness

Figure 6 shows the effects of pulse energy on the average surface roughness. The other two laser parameters, pulse duration and pulse repetition rate, are fixed at 5 ps and 2200 Hz, respectively. As the pulse energy increases, the average surface roughness appears to increase as a logarithmic function. When the pulse energy increases from 50 µJ to 225 µJ, there appears to be a more significant change in the average surface roughness compared to when the pulse energy increases from 225 µJ to 400 µJ.

Figure 7 shows the effects of pulse duration on the average surface roughness. The other two laser parameters, pulse energy and pulse repetition rate, are fixed at 225 µJ and 2200 Hz, respectively. As the pulse duration increases, the average surface roughness appears to decrease as an exponential or linear function. As the pulse duration increases from 0.184 ps to 5 ps, the average surface roughness decreases faster than when the pulse duration increases from 5 ps to 10 ps. The results indicate a relationship between the pulse duration and the average surface roughness values. Compared to the pulse energy, the pulse duration appears to have more influence on the microstructure when looking at the average surface roughness value.

Figure 8 shows the effects of pulse repetition rate on average surface roughness. The other two laser parameters, pulse energy and pulse duration, are fixed at 225 µJ and 5ps, respectively. As the pulse repetition rate increases, the average surface roughness increases almost as a linear function. The results indicate a strong relationship between the pulse repetition rate and the average surface roughness value. Of the three laser parameters (pulse energy, pulse duration, and pulse repetition rate), pulse repetition rate seems to have the most substantial relationship to the average surface roughness value.

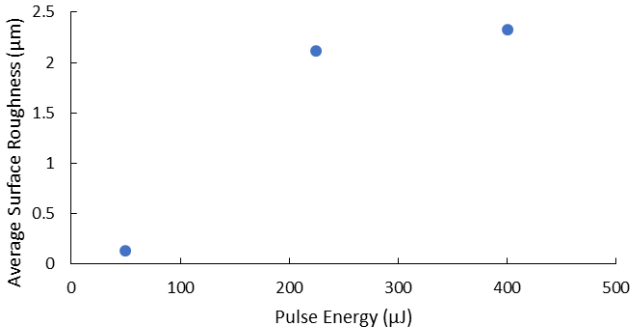

FIGURE 6: EFFECTS OF PULSE ENERGY ON SURFACE ROUGHNESS

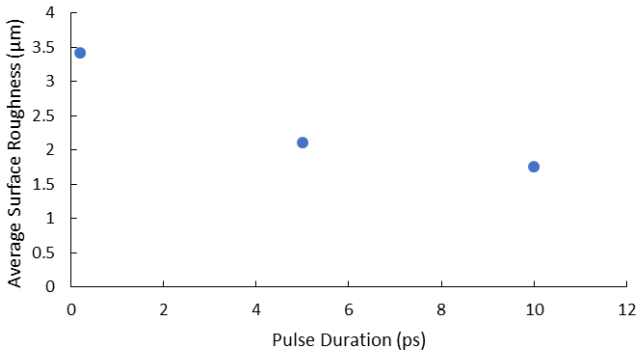

FIGURE 7: EFFECTS OF PULSE DURATION ON SURFACE ROUGHNESS

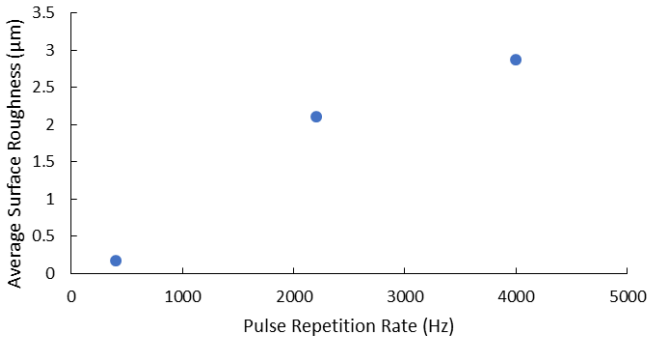

FIGURE 8: EFFECTS OF PULSE REPETITION RATE ON SURFACE ROUGHNESS

3.3 Effects of Laser Parameters on Contact Angle

Figure 9 shows the effects of pulse energy on contact angle. The other two laser parameters, pulse duration and pulse repetition rate, are fixed at 5 ps and 2200 Hz, respectively. As the pulse energy increases, the contact angle appears to increase first before leveling off at high pulse energy values. When the pulse energy increases from 50 µJ to 225 µJ, the increase in

© 2023 by ASME

contact angle is over 40°, and the contact angle remains almost the same when the pulse energy increases from 225 μJ to 400 μJ.

Figure 10 shows the effects of pulse duration on contact angle. The other two laser parameters, pulse energy and pulse repetition rate, are fixed at 225 μJ and 2200 Hz, respectively. As the pulse duration increases, the contact angle increases nonlinearly for the range of pulse duration used, at a higher rate from 0.184 to 5 ps than from 5 to 10 ps.

Figure 11 shows the effects of pulse repetition rate on contact angle. The other two laser parameters, pulse energy and duration, are fixed at 225 μJ and 5ps, respectively. When the pulse repetition rate increases the contact angle increases nonlinearly, and the behavior is similar to the effect of pulse energy. It seems as if it is following a logarithmic trend; when the pulse repetition rate increases from 400 Hz to 2200 Hz, the difference between the two contact angles is more significant than when the pulse repetition rate increases from 2200 Hz to 4000 Hz, having a reduced difference.

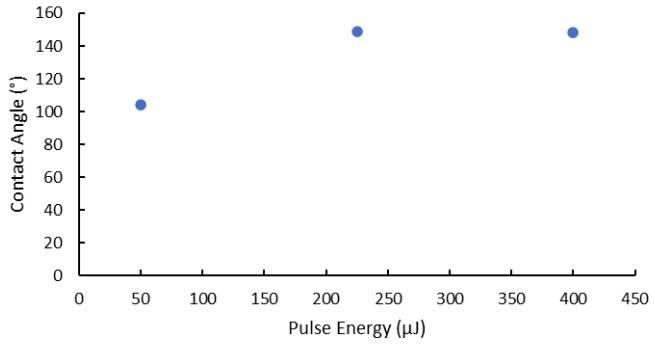

FIGURE 9: EFFECTS OF PULSE ENERGY ON CONTACT ANGLE

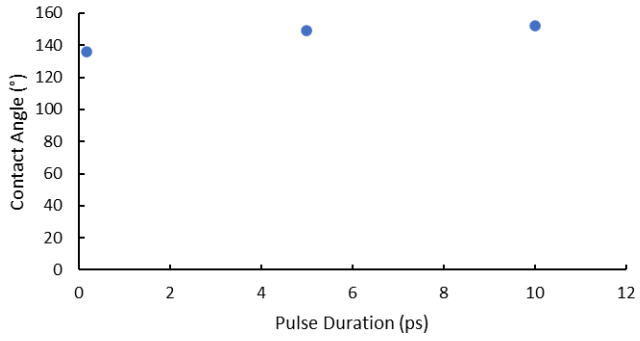

FIGURE 10: EFFECTS OF PULSE DURATION ON CONTACT ANGLE

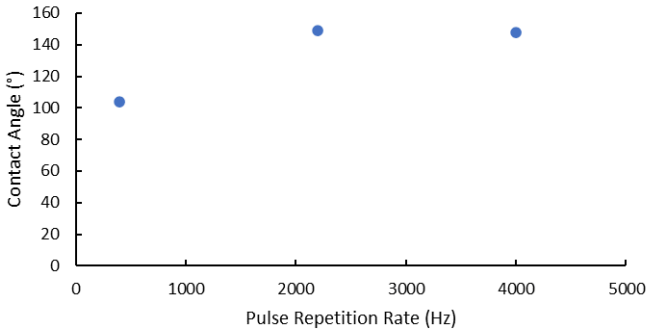

FIGURE 11: EFFECTS OF PULSE REPETITION RATE ON CONTACT ANGLE

3.4 Effects of Surface Roughness on Contact Angle

Figure 12 shows the effect of the average surface roughness on contact angle, after annealing, treating the surface roughness as an independent variable. All samples show hydrophobic results regardless of the average surface roughness. The results suggest that when the average surface roughness is 0.5 μm or less, the average contact angle is hydrophobic, and when the average surface roughness is more significant than 1.5 μm, the contact angle is more likely to exhibit superhydrophobic results. Aside from the observation mentioned, there does not seem to be a clear and direct trend when comparing the average surface roughness to the contact angles, but an optimal surface roughness seems to exist to maximize the contact angle.

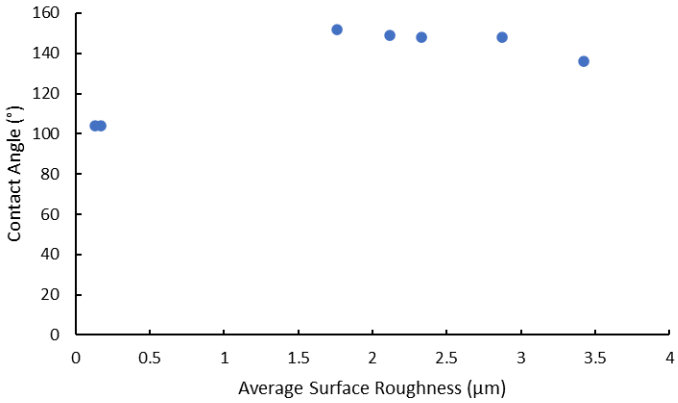

FIGURE 12: EFFECTS OF SURFACE ROUGHNESS ON CONTACT ANGLE

3.5 Response Surface Model

The results of contact angle for all the 20 test runs are shown in Table 3. Through the analysis in SAS software, a response surface model for the contact angle in favor of the factor levels (E, fp, tp) is obtained. The model can be described by the following equation:

© 2023 by ASME

$$\theta = 54.7 + 0.42E + 0.03f_p - 4.9 \times 10^{-5}E^2 - 4.8 \times 10^{-5}Ef_p - 3.9 \times 10^{-6}{f_p}^2 \quad (1)$$

TABLE 3 EXPERIMENTAL DESIGN AND RESULTS

Run Order	E (μJ)	tp (ps)	fp (Hz)	Contact angle (°)
1	50	5	2200	120
2	330	2	1130	157
3	225	5	4000	154
4	120	8	3270	150
5	225	5	2200	161
6	225	5	2200	148
7	120	2	3270	160
8	225	0.184	2200	158
9	225	5	400	132
10	400	5	2200	161
11	225	5	2200	160
12	225	5	2200	160
13	330	8	1130	150
14	330	8	3270	161
15	330	2	3270	156
16	225	5	2200	152
17	225	5	2200	159
18	120	2	1130	131
19	225	10	2200	158
20	120	8	1130	157

Analysis of variance (ANOVA) indicates that the model is highly statistically significant (p-value <0.0001). The coefficient of determination (the ratio of the explained variation to the total variation) R^2 equals 0.80. The R^2 value suggests that the response surface model could provide good predictions. The lack-of-fit test shows that the lack-of-fit (p-value=0.1884) was insignificant, indicating that the model fits well with the experimental data. The response surface model explicitly relates contact angle to laser parameters. Contact angle can be predicted from the response surface model if the laser parameters are varied within the tested experimental ranges in this study.

3.6 Optimization of Laser Parameters

Minitab is used to obtain a multiple response optimization. The response goal is to maximize contact angle. The solution is shown in Table 4.

To compare the results achieved from the model with experiments, additional confirmation experiments are conducted under the following laser parameter setting: pulse energy at 214 μJ, tp at 10 ps, and fp at 2427 Hz. As shown in Table 5, the contact angle obtained from the confirmation experiments is very close to that estimated by the RSM model, implying that the RSM approach is appropriate for optimizing the laser parameters to maximum contact angle.

TABLE 4 OPTIMAL SETTINGS OF LASER PARAMETERS AND PREDICTED VALUES

Optimal setting			Predicted value
E (μJ)	tp (ps)	fp (Hz)	Contact angle (°)
214	10	2427	161

TABLE 5 RESULTS OF CONFIRMATION EXPERIMENTS

Value	Laser parameter			Response
	E (μJ)	tp (ps)	fp (Hz)	Contact angle (°)
Experimental	214	10	2427	168
Predicted	214	10	2427	161
Error (%)				4.3

4. CONCLUSIONS

Surface roughness, microstructure, and contact angle are investigated for laser textured Al6061 samples. The response surface method predicts optimal laser parameters to maximize contact angle. The findings from this work are summarized below:

- Laser surface texturing can generate random roughness and regular patterns on Al6061 samples covering a wide range of roughness values with various multiscale geometric features from hundreds of μm to submicron sizes.
- Surface roughness increases nonlinearly with pulse energy and pulse repetition rate, and the effect is more significant for repetition rate. Surface roughness decreases slowly with pulse duration.
- All three laser parameters have a positive relationship with contact angle. A 12% increase in contact angle is recorded for pulse duration from 0.184 to 10 ps. Pulse energy and repetition rate show a stronger effect on contact angle, with a >40% increase over the range investigated.
- Surface roughness has a significant effect on contact angle. There seems to be an optimal roughness value around 2 μm for maximizing the contact angle.
- Annealing turns the laser textured surface from being hydrophilic to hydrophobic.
- A response surface model for Al6061 establishes the relationship from the contact angle to pulse energy and pulse repetition rate. A maximum contact angle of 161° is predicted with optimal conditions of E=214 μJ, tp=10 ps, and fp=2427 Hz, which agrees well with that from the confirmation test.

ACKNOWLEDGEMENTS

© 2023 by ASME

This work is funded by the Department of Energy's Kansas City National Security Campus, operated by Honeywell Federal Manufacturing & Technologies, LLC, under contract number DE-NA0002839. Partial support by the National Science Foundation (NSF) under Grant No. CMMI-1903740 is gratefully acknowledged.

REFERENCES

[1] Fan, P., Tan, R., and Zhong, M. "Ultrafast laser enabling hierarchical structures for versatile superhydrophilicity with enhanced Cassie-Baxter stability and durability." Langmuir Vol. 35 (2019): pp. 16693-16711.

[2] Ahmmed, K., Ling, E., Servio, P., Kietzig, A. "Introducing a new optimization tool for femtosecond laser-induced surface texturing on titanium, stainless steel, aluminum and copper." Optics and Laser in Engineering Vol. 66 (2015): pp 258-268.

[3] Vorobyev, A.Y., and Guo, C. "Laser turns silicon super wicking." Optics Express Vol. 18 No. 7 (2010): pp. 6455-6460.

[4] Guerrero-Vaca, G., Rodríguez-Valverde, M.A., Castilla-Montilla, P., Alguacil-Salamanca, F., Rodríguez-Alabanda, O., Romero, P.E., Molero-Romero, E., and Ruiz-Cabello, F.J.M. "Superhydrophobic cerium-based coatings on Al-Mg alloys and aluminized steel." Coatings Vol. 9 No. 12 (2019): art. no. 774.

[5] Kostal, E., Stroj, S., Kasemann, S., Matylitsky, V., Domke, M. "Fabrication of Biomimetic Fog-Collecting Superhydrophilic-Superhydrophobic Surface Micropatterns Using Femtosecond Lasers." Langmuir Vol. 34 No. 9 (2018): pp.2933-2941.

[6] Vorobyev, A.Y., and Guo, C. "Multifunctional surfaces produced by femtosecond laser pulses." Journal of Applied Physics Vol. 117 No. 3 (2015): 033103.

[7] Skoulas, E., Manousaki, A., Fotakis, C., and Stratakis, E. "Biomimetic surface structuring using cylindrical vector femtosecond laser beams." Scientific Reports Vol. 7 (2017): pp. 45114-45125.

[8] Kunz, C., Müller, F.A., and Gräf, S. "Multifunctional hierarchical surface structures by femtosecond laser processing." Materials Vol. 11 No. 5 (2018): 789.

[9] Ngo, C.V. and Chun, D. "Fast wettability transition from hydrophilic to superhydrophobic laser-textured stainless-steel surfaces under low-temperature annealing." Applied Surface Science Vol. 409 (2017): pp. 232-240.

[10] Liu W., Cai, M., Luo, X., Chen, C., Pan, R., Zhang, H., and Zhong, M. "Wettability transition modes of aluminum surfaces with various micro/nanostructures produced by a femtosecond laser." Journal of Laser Applications Vol. 31 (2019): 022503.

[11] National Institute of Standards and Technology. "Central Composite Designs (CCD)." https://www.itl.nist.gov/div898/handbook/pri/section3/pri3361.htm. Accessed October, 2022.

[12] Sanders, R. "Technology Innovation in Aluminum Products." JOM: the Journal of the Minerals, Metals & Materials Society Vol. 53 No. 2 (2001): pp. 21-25.

[13] Alcoa Engineered Products. "Understanding Extruded Aluminum Alloys." https://sites.astro.caltech.edu/sedm/_downloads/4c62586a69bdc57ca49a938a3e3fc082/Extruded_Alloy_6061.pdf. Accessed October, 2022.

 © 2023 by ASME